Square-Wave Spatial Optical Orthogonal Frequency-Division Multiplexing

Mohammed S. A. Mossaad, Kaichen Su, Warren Pawlikowski, Zhenyu Charlus Zhang, *Member, IEEE*, Steve Hranilovic, *Fellow, IEEE*, and Lutz Lampe, *Senior Member, IEEE*

***Abstract*—Visible light communication (VLC) systems leverage illumination devices, such as light-emitting diodes (LEDs), to serve a dual role as indoor high-speed communication downlinks. Though high data rates are possible using orthogonal frequency-division (OFDM) in VLC systems, the impact on the complexity and luminous efficacy of the luminaire remain among the key challenges. In this paper, *square-wave spatial optical OFDM* (SW-SO-OFDM) is proposed which transmits an OFDM signal using G square-wave subcarriers from G LED groups and allowing them to sum in space. Using a binary-level square-wave carrier signal eliminates the need for digital-to-analog conversion, non-linear pre-distortion hardware and the transmitter inverse Fourier transform, thereby greatly reducing the complexity of the transmitter in the luminaire. Further, by coordinating the binary transmissions from pairs of LED groups, SW-SO-OFDM can transmit multi-level constellations, which further improves the bandwidth efficiency. Through simulation and experiment, SW-SO-OFDM is shown to provide communication performance comparable to SO-OFDM and to significantly outperform conventional DC-biased (DCO)-OFDM at high signal-to-noise ratios, while considerably reducing the overall transmitter complexity in the luminaire.**

***Index Terms*—Intensity modulation, optical OFDM, visible light communications.**

I. Introduction

VISIBLE light communication (VLC) systems utilize existing lighting devices (i.e., LEDs), to enable high-speed communication in the range from 100 s of Mbps and beyond [1]. The migration of illumination to LEDs due to their higher power efficiency has resulted in the growing interest into complementary VLC applications [2].

Simple and cost-effective VLC systems use intensity modulation/direct detection (IM/DD) [3], [4], [5], by modulating the light source intensity with the information signal and using a simple photodetector at the receiver to directly convert the received optical signal into an electrical current. While various modulation techniques, such as on-off keying (OOK) and pulse-position modulation (PPM), have been proposed for IM/DD-based VLC systems, orthogonal frequency-division multiplexing (OFDM) offers a high spectral efficiency, robustness against multipath dispersion and ease of channel estimation and equalization in time-varying environments [6]. These advantages have led to the widespread adoption of OFDM in numerous communication systems, ranging from radio frequency (RF) applications to fiber and millimeter-wave (MMW) wireless and free-space optics (FSO) [7], [8].

Various techniques have been proposed to adapt OFDM to IM/DD, including DC-biased Optical OFDM (DCO-OFDM) and Asymmetrically-Clipped Optical OFDM (ACO-OFDM) [9]. The most common approach, DCO-OFDM imposes Hermitian symmetry on the OFDM frame and adds a DC bias. The resulting signal is then clipped at zero to ensure that it is non-negative and real and hence suitable for IM/DD channels. High peak-to-average power ratio (PAPR) is an inherent problem in optical OFDM systems [10]. Since the dynamic range of the LED is limited, parts of the signal are clipped, causing non-linear clipping distortion and a bit-error rate (BER) penalty [11]. In particular for illumination systems, the high PAPR DCO-OFDM signal has been shown to reduce the luminous efficacy of the luminaire [12] and reduce the driver energy efficiency [13].

Spatial Optical OFDM (SO-OFDM) was proposed in [14] to combat the high PAPR of OFDM signals. The key concept behind SO-OFDM is a frequency-to-space mapping achieved by the allocation of a subset of OFDM subcarriers to separate groups of LEDs in the luminaire and the summing in space of the signals from different LEDs. Wideband, high PAPR OFDM signals are thus partitioned into many low-PAPR narrowband signals that are transmitted from multiple LEDs. The signals from different LEDs are allowed to sum in space before being detected by a conventional OFDM receiver.

In the simplest form of SO-OFDM, explored in [12], [15], [16], each LED group is assigned a different OFDM subcarrier. In this case, the time-domain OFDM signal of each group is a sinusoidal signal with a PAPR of only 3 dB. In general, SO-OFDM requires a large number of LED groups, in order to achieve a low PAPR and BER at high signal-to-noise ratio (SNR). Note that each group requires a transmit chain consisting of an inverse fast Fourier transform (IFFT), a digital-to-analog converter (DAC), and digital predistortion device (DPD) and an analog driver, which add considerably to overall complexity of

Manuscript received 25 October 2023; revised 23 January 2024; accepted 28 January 2024. Date of publication 6 February 2024; date of current version 27 February 2024. *(Corresponding author: Steve Hranilovic.)*

Mohammed S. A. Mossaad, Kaichen Su, Warren Pawlikowski, Zhenyu Charlus Zhang, and Steve Hranilovic are with the Department of Electrical and Computer Engineering, McMaster University, Hamilton, ON L8S 4L8, Canada (e-mail: abdullms@mcmaster.ca; suk4@mcmaster.ca; pawlikws@mcmaster.ca; charlus.zhang@mcmaster.ca; hranilovic@mcmaster.ca).

Lutz Lampe is with the Department of Electrical and Computer Engineering, University of British Columbia, Vancouver, BC V6T 1Z4, Canada (e-mail: lampe@ece.ubc.ca).

Digital Object Identifier 10.1109/JPHOT.2024.3362348

the SO-OFDM system. One approach to reducing the hardware complexity of SO-OFDM is to combine it with other PAPR reduction techniques (e.g., pilot-assisted PAPR reduction) [17]. However, this comes at the expense of increased computational complexity.

To reduce complexity, several recent approaches have considered using spatial summing to modulate multiple LEDs with binary-level signals to produce complex modulation. Du et al. [18] use a spatial summing architecture to construct a multilevel pulse-amplitude modulation (PAM) signal at the receiver from the spatial superposition of multiple on-off keying (OOK) signals from multiple transmitters. A similar approach was employed by Kong et al. to generate a 4-PAM signal from OOK signals in an underwater wireless optical communication setting [19]. In [20], a bipolar optical OFDM signal was converted into a binary pulse time modulation (PTM) signal for switching the LEDs on and off, thereby reducing the PAPR of the original OFDM signal and combatting the LED nonlinearity. In [21], which extends the earlier work in [22], binary signals are used to modulate individual LEDs and the spatial summing property of VLC channels is used to superimpose the low-rate binary signals onto a single high-rate optical signal at the receiver. However, the discussion in [21] is limited to variations of PAM signals and the superposition of multiple binary streams to reduce the PAPR of OFDM signals is not discussed. DAC-less transmission has also been explored for other communication systems, such as optical fiber communication. For example, [23] employed two binary signals to drive a Mach-Zehnder modulator to produce a 4-PAM signal. Recently, a digital-to-light converter (DLC) has been proposed by Yang et al. [24], enabling the transmission of an OFDM signal constructed by the superposition of 255 binary signals from 255 distinct LEDs.

In this paper, we propose *square-wave spatial optical OFDM* (SW-SO-OFDM) which transmits a single subcarrier per LED group by modulating an on/off square wave carrier rather than a sinusoid. That is, each LED group is assigned a specific subcarrier frequency and the signal emitted from each LED group is a binary square-wave carrier where data are transmitted by phase-shift keying (PSK). Unlike [24], where a traditional OFDM frame is transmitted using an optical DAC consisting of many LEDs, our approach directly modulates LEDs and is lower in complexity. Our approach also differs from [20], where the OFDM signal does not modulate the LEDs directly, but is converted to a binary PTM signal to eliminate the need for DACs. While the idea of DAC-less transmission and the concept of spatial summation for indoor VLC systems have been studied before in literature [12], [18], [19], [23], and applied to OFDM [20], [24], to our knowledge, this is the first paper to propose using square-wave carriers for OFDM-based VLC systems to enable DAC-less transmission and simplify the transmitter design. Furthermore, we extend SW-SO-OFDM and present a new multi-level signaling approach by coordinating the transmission of two (or more) LEDs to generate multi-level quadrature amplitude modulation (QAM) constellations using only binary-level carriers. This *coordinated* SW-SO-OFDM (C-SW-SO-OFDM) approach is shown both in simulation and experiment to enable the transmission of large QAM constellations without the need for a DAC and using only binary level waveforms.

The remainder of this paper is organized as follows. In Section II, the indoor VLC channel model and considerations such as LED nonlinearity and its impact on the luminous efficacy of signaling LEDs are described. Section III details the basic SW-SO-OFDM transmitter architecture and provides a bit-error probability analysis. In Section III-D, C-SW-SO-OFDM is introduced that allows for multi-level signaling by coordinating the binary level transmissions of pairs of LED groups to produce a complex QAM constellation point. In Section IV, SW-SO-OFDM is compared to other techniques such as the conventional DCO-OFDM and SO-OFDM in terms of BER, obtained both analytically and through Monte-Carlo simulations. Section V provides a detailed description of an experimental validation of C-SW-SO-OFDM technique. Finally, conclusions and future directions are discussed in Section VI.

II. System Modelling

In this section, key system modeling parameters are introduced necessary to consider design of VLC OFDM (cf. [12, Sec. II] for more background).

A. Indoor VLC Channel Model

The LEDs in the luminaire are modeled as having a Lambertian emission pattern. Since in a typical indoor VLC setting, the distance d between the luminaire and the receiver photodetector (on the order of a few meters) is at least two orders-of-magnitude larger than the distance between individual LEDs in the luminaire (on the order of a few centimeters), a reasonable assumption to make is that the optical propagation channels between all LEDs and the receiver photodetector are nearly identical (following [12]). Though the line-of-sight component dominates, practical VLC scenarios also include dispersion from multipath reflections from the ceiling and walls [4], [25]. The DC gain of indoor VLC channel in the passband is modeled as

$$\Omega = \begin{cases} \frac{(m+1)A_{\mathrm{d}}}{2\pi d^2} \cos^m(\phi) T_{\mathrm{s}}(\psi) g(\psi) \cos(\psi), & 0 \leq \psi_{\leq} \psi_{\mathrm{c}} \\ 0, & \psi > \psi_{\mathrm{c}} \end{cases} \tag{1}$$

where m is the Lambertian order, A_{d} is the area of the detector, ψ is the angle of incidence, ϕ is the angle of irradiance, $T_s(\psi)$ is the gain of the optical filter, $g(\psi)$ is the gain of the optical concentrator, and ψ_{c} is the field-of-view (FOV) of the receiver.

The optical power received by the photodetector is the sum of the optical power from the L LEDs of the luminaire

$$P_{\mathrm{R}} = L\Omega P_{\mathrm{T}}, \tag{2}$$

where P_{T} is the optical power output of an LED.

B. LED Nonlinearity

The relation between the luminous flux output ϕ_{v} [lm] and the LED current I [mA] is nonlinear, and typically provided in datasheets. For a popular illumination LED, a quadratic fit to the

characteristics specified in the datasheet [26] is given by [27]

$$\phi_{\mathrm{v}}\ (\mathrm{lm}) = -0.0001I^2 + 0.3093I + 3.647, \tag{3}$$

where I is the instantaneous LED current in mA. The conversion factor between the luminous flux and the radiated optical power for this setup has been evaluated at $2.1\ \mathrm{mW/lm}$ [28].

Since the OFDM signal has large peaks, hard-clipping is necessary for the driving LED current I to fit within the limited dynamic range of the LED. The upper and lower LED current clipping levels are denoted by I_{u} and I_{l}, respectively. In case of symmetric clipping, used throughout this paper, $I_{\mathrm{u}} = -I_{\mathrm{l}} = C$, where C is half the dynamic range. Note that the time-domain OFDM signal before the addition of the DC bias has a zero mean. Therefore, the lower clipping level I_{l} is negative.

For conventional DCO-OFDM and spatial optical OFDM (SO-OFDM) [12], a DPD is required for each LED group to linearize the relation between I and P_{T} [12]. Accordingly, a linear relation between the instantaneous optical power output, P_{T}, and the OFDM signal current, I, is achieved, where the LED conversion factor in $(\mathrm{W/A})$ is denoted by S. In addition, an IFFT block and a DAC are needed for each LED group. As will be described in Section III, SW-SO-OFDM does not require a DPD or DAC converter since it emits only binary waveforms.

C. Impact of Modulation on Luminous Efficacy

The DC current driving the LEDs in a luminaire determines the average luminous flux output ϕ_{v} (lm) or illuminance E (lx) at a surface. Throughout this paper, a DC current level of $500\ \mathrm{mA}$ is considered, unless otherwise indicated. In a VLC system, a modulating current is imposed onto the DC driving current. The *luminous efficacy* is defined as the ratio of the average luminous flux of the LED to the electrical power consumed by the LED. For a given average current, modulating the LED with a time varying signal reduces the luminous efficacy of an LED [12], [26], [27]. The luminous efficacy is an important parameter in lighting as it quantifies how well the LED converts electrical power into useful illumination. The relative luminous efficacy, η_{rel} is defined as the ratio of the luminous efficacy of communication LEDs to that of LEDs driven by a DC current.

In this work, the relative luminous efficacy is defined as the ratio of the time average of the luminous flux output to the electrical power consumed by the LED, i.e.,

$$\eta_{\mathrm{rel}} = \frac{\int_{\langle T_{\mathrm{sym}}\rangle} \phi_{\mathrm{v}}(t)dt \,/\, \int_{\langle T_{\mathrm{sym}}\rangle} P_{\mathrm{LED}}(t)dt}{\eta_{\mathrm{DC}}}, \tag{4}$$

where T_{sym} is the OFDM symbol duration and η_{DC} is the DC luminous efficacy. In contrast to [12], the definition (4) does not make a Gaussian assumption on the distribution of the modulating signal and is appropriate in the case when few or a single subcarriers is modulated per LED group.

Fig. 1 presents a contour plot of the relative luminous efficacy (η_{rel}) computed using (4) for SO-OFDM using a single sinusoidal subcarrier per LED group. The root mean square (RMS) value (σ_g) of the time-domain signal before clipping, $x_g(t)$, defined as

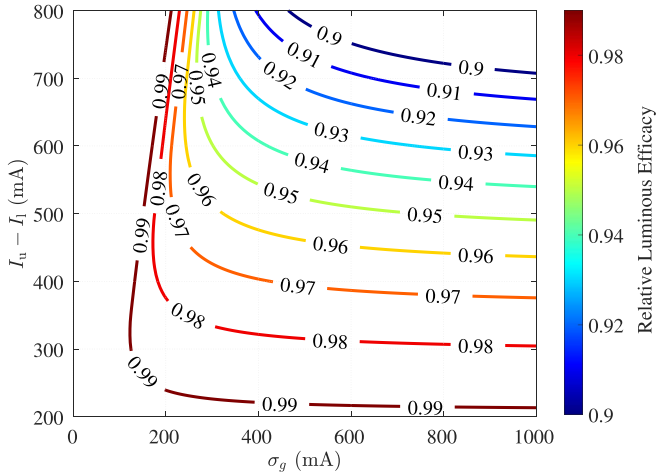

Fig. 1. Contour plot of the relative luminous efficacy η_{rel} as a function of the signal RMS value (σ_g) [mA] and dynamic range ($I_{\mathrm{u}} - I_{\mathrm{l}}$) [mA].

$$\sigma_g = \sqrt{\frac{1}{T_{\mathrm{sym}}} \int_{\langle T_{\mathrm{sym}}\rangle} x_g^2(t)dt}, \tag{5}$$

is represented on the horizontal axis. The dynamic range ($I_{\mathrm{u}} - I_{\mathrm{l}}$) is represented on the vertical axis. The results show that η_{rel} decreases as either σ_g and ($I_{\mathrm{u}} - I_{\mathrm{l}}$) increases. This is expected since operating at the extremes of the dynamic range incurs more nonlinear distortion (NLD) and causes the luminous efficacy to drop [12]. In Section IV, the definition of relative efficacy in (4) will be employed to provide a fair comparison of SW-SO-OFDM versus SO-OFDM considering illumination constraints.

III. Square-Wave Spatial Optical OFDM

A. Background and Motivation

Conventional OFDM communication systems, which dominate wireless applications such as Wi-Fi and cellular communications, are based on the modulation of multiple orthogonal sinusoidal carriers [29]. Sinusoidal signals are chosen to control the emission spectrum and comply with wireless spectrum management regulations. In contrast, for indoor VLC communication systems, the spectrum is unregulated and unlicensed. This motivates the search for alternative periodic carrier waveforms that balance communication performance, illumination and system complexity.

With the aim of retaining the use of commercially available OFDM receivers (as in the upcoming VLC standard 802.11bb [30]), the receiver in this work is considered to be a conventional OFDM receiver matched to sinusoidal carriers. The focus in this work is on transforming the transmitter design in order to reduce system complexity in the luminaire transmitter by considering alternative carrier signals. Since typical VLC channels have a low-pass frequency response dominated by the slow yellow light component of phosphor-coated white LEDs [28], the higher-frequency harmonics of a periodic carrier signal are likely to be more highly attenuated by the VLC channel than the fundamental. Moreover, the higher-frequency components are

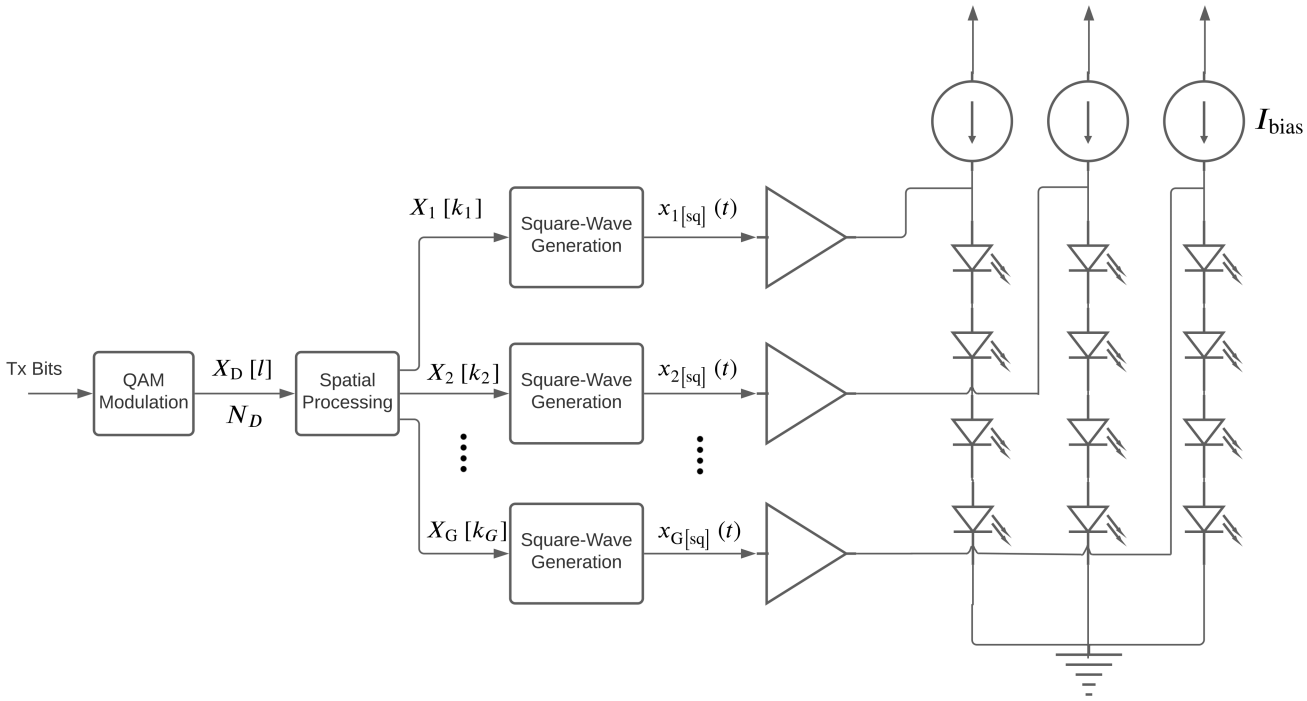

Fig. 2. Architecture of SW-SO-OFDM with G LED groups and $L_g = 4$ LEDs per group.

further attenuated or filtered out by the low-pass anti-aliasing and/or noise rejection filter at the receiver front-end. Therefore, in this work, only the fundamental frequency component is used for detection at the receiver, and its power is defined as the useful signal power, while higher-order harmonic components are considered inter-carrier interference (ICI), and signaling at these harmonic frequencies is avoided. A complete discussion along with methods to avoid the harmonics is provided in Section III-B.

Hence, a parameter of particular interest in assessing periodic carrier waveforms is the fundamental frequency term of the Fourier series (FS) expansion of the periodic signal. In particular, let $p(t)$ denote a periodic signal with fundamental frequency f_0 and restricted to amplitude range $[-C, C]$ in order to avoid nonlinear clipping. Denote the fundamental frequency coefficient of the FS expansion of $p(t)$ as $K_{[p]}$ where

$$K_{[p]} = \frac{2}{T}\int_{-T/2}^{T/2} p(t)\cos(2\pi f_0 t)dt, \tag{6}$$

and $T = 1/f_0$ is the fundamental period of $p(t)$, and without loss of generality and for simplicity, an even signal $p(t)$ is assumed. It is shown in the appendix that of all possible signals $p(t)$ satisfying the amplitude constraints, square waves with a 50% duty cycle have the largest $K_{[p]}$. For 50% duty-cycle square waves, the fundamental coefficient of the FS expansion in (6) is $K_{[\mathrm{sq}]} = 4C/\pi$, while for a sinusoidal wave having an amplitude of C, $K_{[\mathrm{sin}]} = C$. This gives square-wave carriers an SNR advantage of $20\log_{10}(4/\pi) = 2.10$ dB over sinusoidal carriers.

In addition, square-wave carriers are simpler to generate using digital electronic circuits (e.g. by clock division) and do not require a complex DAC as is the case with sinusoidal carriers which are also harder to synchronize [31], [32]. Moreover, since a square wave is a binary-level signal with only two intensity levels, there is no need for a DPD to linearize the output optical power versus input drive current relationship for each LED group in SO-OFDM.

B. Square-Wave Spatial Optical OFDM Definition

The functional block diagram of the SW-SO-OFDM architecture is shown in Fig. 2. The transmitter design is based on the spatial summing architecture, introduced in [12], where the L available LEDs are divided into G LED groups, and the signaling of LEDs in the same group is identical, and allowed to sum in space to produce the desired signal at the receiver. In case of SW-SO-OFDM, however, each LED group is modulated by a binary-level signal. Let G denote the number of groups and L_g denote the number of LEDs in the g-th group, where

$$\sum_{g=1}^{G} L_g = L. \tag{7}$$

As shown in Fig. 2, the data bits are modulated to produce the QAM constellation data symbols, $X_{\mathrm{D}}[l]$, for $l = 1, 2, \ldots, N_{\mathrm{D}}$. The spatial processing block maps the N_{D} data symbols, $X_{\mathrm{D}}[l]$, into G LED-group SW-SO-OFDM symbols

$$X_g[k_g] = |X_g[k_g]|\exp(j\phi_g[k_g]) \tag{8}$$

for $g = 1, 2, \ldots, G$, where k_g is the subcarrier index associated with LED group g and $\phi_g[k_g]$ denotes the angle of $X_g[k_g]$. Given the system bandwidth B_{S} and the subcarrier spacing Δf, such that $B_{\mathrm{S}} = N_{\mathrm{A}}\Delta f$, where N_{A} is the total number of available subcarriers, only a subset of the N_{A} subcarriers are modulated. The modulated subcarriers are indexed by k_g and correspond

to subcarrier frequencies $k_g\Delta f$, for $g = 1, 2, \ldots, G$. For convenience and without loss of generality, the subcarrier indexing is such that $k_1 \leq k_2 \leq \ldots \leq k_G$. Note that the subcarrier indexing does not necessarily start from 1, not all available subcarriers are modulated, and the data-carrying subcarriers indexed by $k_1, k_2, \ldots, k_G$ need not be contiguous. Since only a binary-level square-wave signals are transmitted, $|X_g[k_g]| = 1$ without loss of generality.

Note that the mapping from $X_{\rm D}[l]$ to $X_g[k_g]$ has many degrees of freedom and is not necessarily one-to-one. Generally, a single data symbol $X_{\rm D}[l]$ can be mapped to either one or two or more LED group SW-SO-OFDM symbols $X_g[k_g]$ depending on the SW-SO-OFDM structure used. Hence, in general $G \geq N_{\rm D}$. The mapping can take various forms. In this paper, two mapping techniques are described: the simplest approach, termed *uncoordinated* transmission in Section III-C, performs a one-to-one mapping between X_D and X_g, implying $G = N_{\rm D}$, while a *coordinated* technique, presented in Section III-D coordinates the transmission of two LED groups to represent a complex QAM symbol, implying $G = 2N_{\rm D}$.

The transmitted SW-SO-OFDM signal is given by

$$x_{[\rm sq]}(t) = \sum_{g=1}^{G} x_{g[\rm sq]}(t), \tag{9}$$

where $x_{g[\rm sq]}(t)$ is the binary-level SW-SO-OFDM time-domain signal of the g-th LED group, which is determined by the data symbol $X_g[k_g]$, and is given by

$$x_{g[\rm sq]}(t) = C\,{\rm sq}(2\pi k_g \Delta f t + \phi_g[k_g]), \tag{10}$$

for $0 \leq t \leq T_{\rm sym}$, where $T_{\rm sym}$, the SW-SO-OFDM symbol duration, is the inverse of Δf, which ensures the orthogonality of the continuous-time SW-SO-OFDM signal. The square wave function ${\rm sq}(\cdot)$ is defined as

$${\rm sq}(\chi) = {\rm sgn}(\cos(\chi)). \tag{11}$$

The VLC channel is lowpass due to limited LED bandwidth, multipath distortion in propagation, and the receiver anti-aliasing filter. In order to ease processing at the receiver, as is standard in OFDM systems, a cyclic prefix (CP) should be appended to the OFDM frame.

A DC bias current $I_{\rm bias} \geq C$ is added to the group signal $x_{g[\rm sq]}[n]$ to ensure nonnegativity, and the LEDs in each group are driven by the resulting signal. It is worthwhile to note here that this DC bias is necessary to maintain the target average optical power output of the LEDs, and hence the target illumination level set by lighting requirements. It thus does not constitute an energy efficiency loss for the VLC system.

The optical signals from all LEDs are attenuated by the VLC channel response with a DC optical gain Ω, as described in Section II-A, and are summed spatially at the receiver. The receiver block diagram is shown in Fig. 3. The photodetector, with responsivity R (A/W), converts the received optical sum signal into an electrical signal. The signal is then filtered with an anti-aliasing/noise rejection lowpass filter (LPF). The signal is then sampled with a sampling interval $T_{\rm s}$ and input to the fast Fourier transform (FFT) block of size N. The CP added at the transmitter should be removed from the OFDM frame upon reception and prior to the FFT. The OFDM symbol duration is the product of to the sampling interval and the FFT size ($T_{\rm sym} = NT_{\rm s}$). Finally, the received frequency-domain OFDM symbols produced by the FFT are demodulated and converted to bits.

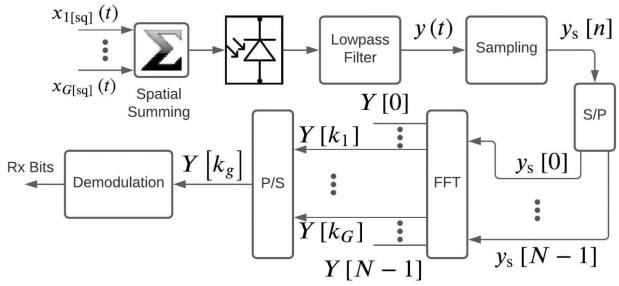

Fig. 3. Spatial summing and architecture of the SW-SO-OFDM receiver. Note that only the subset $\{Y[k_1], \ldots, Y[k_G]\}$ of the set of received OFDM frequency-domain symbols $\{Y[0], Y[1], \ldots, Y[N-1]\}$ is used for demodulation and bit detection.

The received SW-SOFDM signal is given by,

$$\widetilde{x}_{[\rm sq]}(t) = \left(h * x_{[\rm sq]}\right)(t), \tag{12}$$

where $h(t)$ is the impulse response of the VLC channel and the receiver front-end LPF of cut-off frequency $f_{\rm c}$ normalized to have a unity DC gain. Therefore, the output of the receiver LPF can be written as

$$y(t) = \frac{G_{\rm E}L}{G}\widetilde{x}_{[\rm sq]}(t) + G_{\rm E}LI_{\rm bias} + w(t), \tag{13}$$

where $G_{\rm E} = R\Omega S$ is the overall electrical gain of the system and $w(t)$ is the receiver noise waveform. For simplicity, the case of equal numbers of LEDs per group, i.e. $L_g = L/G$ for $g = 1, 2, \ldots, G$, is considered. In the following, the data are assumed to be transmitted on the fundamental-frequency components of the square-wave carriers in the passband of the VLC channel. For convenience, the passband is modelled as having a flat response with gain G_E. Notice that $\widetilde{x}_{[\rm sq]}(t)$ differs from $x_{[\rm sq]}(t)$ (10) in that $\widetilde{x}_{[\rm sq]}(t)$ has higher frequency harmonics attenuated by the VLC channel or filtered out by the receiver LPF. The fundamental-frequency components are equal for both $x_{[\rm sq]}(t)$ and $\widetilde{x}_{[\rm sq]}(t)$ since the DC channel gain Ω already takes into account the VLC channel attenuation suffered by the fundamental-frequency data-carrying subcarriers. Though the passband is assumed flat here for convenience in this analysis, it is straightforward to extend to the case of a non-flat passband. Additionally, the DC bias term is ignored in the following, since it does not carry any information. The filtered received signal, $y(t)$, is then sampled to yield

$$\begin{aligned} y_{\rm s}[n] &= y\left(nT_{\rm s} + \delta\right) \\ &= \frac{G_{\rm E}L}{G}\widetilde{x}_{[\rm sq]}[n] + w[n], \end{aligned} \tag{14}$$

for $n = 0, 1, \ldots, N-1$, where $\delta = d/c$ is the propagation delay from transmitter to receiver, $\widetilde{x}_{[\rm sq]}[n]$ and $w[n]$ are the sampled received SW-SO-OFDM signal and the sampled receiver noise, respectively. The variance of the zero-mean Gaussian-distributed samples $w[n]$ is denoted by σ_w^2.

C. Uncoordinated Transmission

Uncoordinated SW-SO-OFDM (U-SW-SO-OFDM) transmission maps QAM data symbols $X_{\mathrm{D}}[l]$ to the frequency-domain OFDM subcarrier symbols in a one-to-one fashion, i.e., $X_g[k_g] = X_{\mathrm{D}}[g]$ for $g = 1, 2, \ldots, N_{\mathrm{D}}$. In this case the number of LED groups $G = N_{\mathrm{D}}$. Given that $X_g[k_g]$ is restricted to a constant magnitude, the QAM data symbols $X_{\mathrm{D}}[l]$ are also limited to be constant modulus (i.e., PSK constellations).

The received SW-SO-OFDM frequency-domain frame, $Y[k]$ for $k = 0, 1, \ldots, N-1$, is obtained by using the N-point FFT operation. However, only the receiver subcarrier symbols $Y[k_g]$ for $k_g = k_1, k_2, \ldots, k_G$ carry useful QAM data and are demodulated after the FFT operation.

In SW-SO-OFDM, the modulated subcarriers are accompanied by higher frequency harmonics which must also be considered. In this paper, the subcarrier assignment is done so that the fundamental frequencies of the modulated subcarriers are in the passband of the channel. In contrast, higher-order frequency harmonics of the square-wave carriers are either significantly attenuated or filtered out completely by the indoor VLC channel frequency response. Moreover, a lowpass anti-aliasing/noise rejection filter is used at the receiver front end and can be modeled as an ideal LPF with a cut-off frequency $f_{\mathrm{c}} = N_{\mathrm{A}}\Delta f = N_{\mathrm{A}}/T_{\mathrm{sym}}$, and all harmonic frequency components beyond f_{c} are filtered out. Therefore, the higher-order frequency harmonics of the square-wave carriers are not used for detection, do not contribute to the useful signal power, and are considered ICI. In this paper, the subcarrier frequencies occupied by the harmonics are left unmodulated to avoid ICI. Specifically, if the subcarrier indexed by k_g is modulated, then signaling at odd multiples of k_g i.e., $3k_g, 5k_g, \ldots$ are avoided.

Though not considered in this paper, the bandwidth efficiency of SW-SO-OFDM can be improved by modulating data on the odd-multiple harmonics and compensating for ICI using a decoding technique such as successive interference cancelling (SIC). Specifically, since the demodulation of the g-th, $g = 1, \ldots, G$, square wave in U-SW-SO-OFDM only makes use of one subcarrier indexed by k_g, the symbol $X_g[k_g]$ from subcarrier k_g can be estimated while allowing ICI on the harmonics of the g-th square wave. Assuming the estimation of $X_g[k_g]$ is accurate, then the g-th square wave can be reconstructed and removed from the received signal, thus removing the interfering harmonics on the other subcarriers. This leads to a ICI-free demodulation for $g+1$-th square wave. As a result, all available subcarriers can be used for carrying data. While SIC can be computationally expensive, a majority of the computational burden falls on the receiver and not on the luminaire transmitter which must be low complexity to ensure energy efficiency. Additionally, SIC approaches generally suffer from error propagation. Given that VLC channels typically operate at high SNRs, it is anticipated that this impact will not be severe and is left as future work.

Considering that the fundamental components of the square-wave carriers are in the passband of the channel, $Y[k_g]$, the output of the FFT operation for $k_g = k_1, \ldots, k_G$, can be written as

$$Y[k_g] = \mathrm{FFT}\left[y_{\mathrm{s}}[n]\right] = \frac{1}{\sqrt{N}}\sum_{n=0}^{N-1} y_{\mathrm{s}}[n]\exp\left(-j\frac{2\pi k_g n}{N}\right) = \underbrace{\frac{\sqrt{N}G_{\mathrm{E}}K_{[\mathrm{sq}]}L}{2\,G}X_g[k_g]}_{\text{Useful Signal Term}} + \underbrace{W[k_g]}_{\text{Noise Term}}, \tag{15}$$

where $X_g[k_g] = |X_g[k_g]|\exp\left(j\phi_g[k_g]\right) = X_{\mathrm{D}}[g]$, and $W[k_g]$ is the FFT of the receiver noise.

The useful signal power in (15) is defined as

$$\sigma^2_{[\mathrm{sq}]}[k_g] = \frac{N}{4}\left(\frac{G_{\mathrm{E}}K_{[\mathrm{sq}]}L}{G}\right)^2 = 4N\left(\frac{G_{\mathrm{E}}LC}{\pi G}\right)^2, \tag{16}$$

where the second equation follows by substituting $K_{[\mathrm{sq}]} = 4\,C/\pi$. Hence, the SNR per subcarrier channel is

$$\mathrm{SNR}_{[\mathrm{sq}]}[k_g] = \frac{\sigma^2_{[\mathrm{sq}]}[k_g]}{\sigma^2_W} = \frac{N\left(G_{\mathrm{E}}K_{[\mathrm{sq}]}L/G\right)^2}{4\sigma^2_W} = 4N\left(\frac{G_{\mathrm{E}}LC}{\pi G\sigma_W}\right)^2, \tag{17}$$

where $\sigma^2_W = \mathrm{E}(|W[k_g]|^2) = \sigma^2_w$.

For M-PSK modulation, to which SW-SO-OFDM is restricted given the use of fixed-intensity LED signals, the bit error probability for the data modulated on the k_g-th subcarrier can be approximated as [33]

$$P_{\mathrm{e}[\mathrm{sq}]}[k_g] \approx \frac{1}{\log_2 M}\mathrm{erfc}\left(\sin\left(\frac{\pi}{M}\right)\sqrt{\mathrm{SNR}_{[\mathrm{sq}]}[k_g]}\right). \tag{18}$$

Under the assumption that all subcarriers have the same SNR, the overall BER is given by the same expression (18). Therefore, for $M = 4$, the BER can be written as

$$P_{\mathrm{e}[\mathrm{sq}]} \approx \frac{1}{2}\mathrm{erfc}\left(\frac{\sqrt{2N}G_{\mathrm{E}}LC}{\pi G\sigma_W}\right). \tag{19}$$

Notice that SW-SO-OFDM does not suffer from any NLD clipping noise, which is a major advantage over conventional DCO-OFDM, since VLC systems operate at high SNRs where the effect of NLD clipping noise is dominant over that of receiver additive white Gaussian noise (AWGN). Moreover, SW-SO-OFDM offers the advantage of a simpler transmitter architecture compared to SO-OFDM and DCO-OFDM. Moreover, SW-SO-OFDM offers the advantage of a simpler transmitter architecture compared to SO-OFDM and DCO-OFDM. Table I compares the hardware complexity of DCO-OFDM, SO-OFDM, and SW-SO-OFDM. The computational complexities of DPDs, DACs, and spatial filters are denoted by $\mathcal{DPD}(\cdot)$, $\mathcal{DAC}(\cdot)$, and $\mathcal{S}(\cdot)$, respectively. Table I shows that SW-SO-OFDM has lower hardware and computational complexity than both DCO-OFDM and SO-OFDM since it eliminates the need for DACs, DPDs, IFFTs, and spatial filters. Section IV presents a BER comparison of DCO-, SO- and SW-SO-OFDM. Section IV presents a BER comparison of DCO-, SO- and SW-SO-OFDM.

TABLE I
COMPARISON OF TRANSMITTER HARDWARE AND COMPUTATIONAL COMPLEXITY OF DCO-OFDM, SO-OFDM, AND SW-SO-OFDM

Modulation technique	Hardware complexity	Computational complexity
DCO-OFDM	1 IFFT, 1 DPD, and 1 DAC.	$\mathcal{O}\left(N\log_2\left(2N_{\mathrm{D}}\right)\right)+\mathcal{DPD}(N)$ $+\mathcal{DAC}(N)$
SO-OFDM	G Spatial Filters, G IFFTs, G DPDs, and G DACs.	$G\left(\mathcal{O}\left(N\log_2\left(2\epsilon\right)\right)+\mathcal{DPD}(N)\right.$ $\left.+\mathcal{DAC}(N)+\mathcal{S}(N)\right)$
SW-SO-OFDM	Generation of G square waves from QAM data.	No IFFT required.

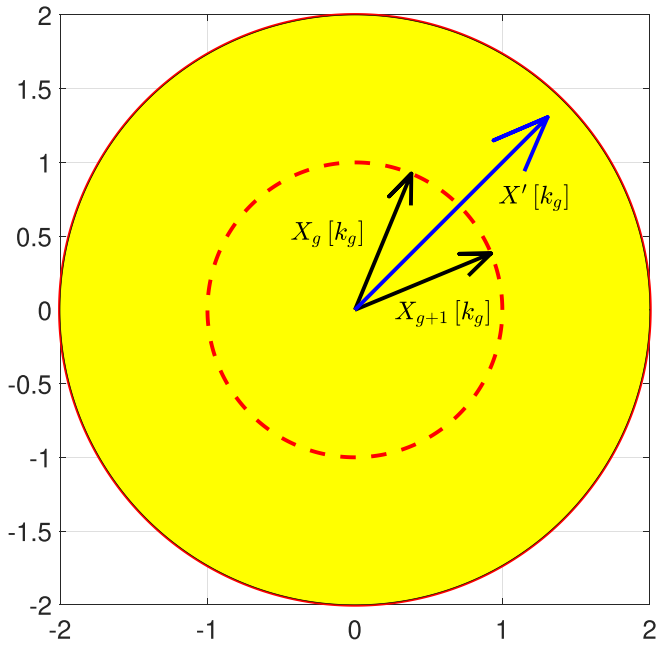

Fig. 4. Phasor diagram showing how two signals with the same fixed intensity level can be added the same way as vector addition, to give a resultant signal in the intensity range from 0 to double the original intensity.

D. Coordinated Transmission

A clear disadvantage of U-SW-SO-OFDM in Section III-C is that using square-wave carriers with fixed intensity level for each LED restricts the QAM constellations to be constant modulus (i.e., PSK). In this section, Coordinated SW-SO-OFDM (C-SW-SO-OFDM) is introduced, which preserves the simple transmitter architecture introduced in Section III, but allows for multi-level QAM signaling by coordinating the binary-level transmissions of pairs of LEDs. In contrast to U-SW-SO-OFDM where the mapping between the QAM constellation data symbols $X_{\mathrm{D}}[l]$ and the LED group SW-SO-OFDM subcarrier symbols $X_g[k_g]$ is one-to-one, for C-SW-SO-OFDM, each data symbol is mapped to two group subcarrier symbols signaling at the same frequency. Hence, for C-SW-SO-OFDM, double the number of LED groups is required for C-SW-SO-OFDM compared to U-SW-SO-OFDM, i.e., $G=2N_{\mathrm{D}}$. In particular, in this Section the transmissions from pairs of LEDs indexed by g and $g+1$ (where $g=1,3,5,\ldots,G-1$) are coordinated.

The phasor diagram in Fig. 4 demonstrates how a multi-level constellation can be constructed from two fixed-intensity signals. Consider two constant-modulus LED group signals $X_g[k_g]=\exp(j\phi_g[k_g])$ and $X_{g+1}[k_g]=\exp(j\phi_{g+1}[k_g])$ (represented by black arrows in the figure) from groups g and $g+1$ respectively. The fixed magnitude of $X_g[k_g]$ and $X_{g+1}[k_g]$ (represented by the red dotted circle) is normalized to 1, without loss of generality (since the square-wave group signals $x_g(t)$ and $x_{g+1}(t)$ are scaled to have a fixed amplitude C). By coordinating the emissions from $X_g[k_g]$ and $X_{g+1}[k_g]$ (i.e., $\phi_g[k_g]$ and $\phi_{g+1}[k_g]$), the resultant QAM data symbol, $X'[k_g]=|X'[k_g]|\exp(j\phi'[k_g])$ (represented by a blue arrow in the figure) is generated. In particular, assuming groups g and $g+1$ are adjacent their intensities sum in space giving rise to the intensity sum signal $X'[k_g]$

$$\begin{aligned}X'[k_g]&=X_g[k_g]+X_{g+1}[k_g]\\&=|X'\,[k_g]|\exp\left(j\phi'\,[k_g]\right)\\&=\exp\left(j\phi_g[k_g]\right)+\exp\left(j\phi_{g+1}[k_g]\right).\end{aligned}\tag{20}$$

Notice that

$$|X'[k_g]|=2\left|\cos\left(\frac{\Delta\phi[k_g]}{2}\right)\right|.\tag{21}$$

where $\Delta\phi[k_g]=\phi_g[k_g]-\phi_{g+1}[k_g]$ and

$$\phi'[k_g]=\angle X'[k_g]=\frac{\phi_g[k_g]+\phi_{g+1}[k_g]}{2}.\tag{22}$$

Hence, with the proper selection of $\phi_g[k_g]$ and $\phi_{g+1}[k_g]$, any QAM constellation point in the normalized magnitude range of $0\le|X'[k_g]|\le 2$ can be obtained as the resultant QAM data symbol $X'[k_g]$. Thus, given a target QAM data symbol $X_{\mathrm{D}}[l]$, such that $0\le|X_{\mathrm{D}}[l]|\le 2$, the LED group symbols $X_g[k_g]$ and $X_{g+1}[k_g]$ used to construct $X'[k_g]$ so as to ensure that $X'[k_g]=X_{\mathrm{D}}[l]$, can be obtained by application of (21) and (22).

Following the same steps as outlined in Section III-C, for C-SW-SO-OFDM, the output of the FFT operation for subcarrier k is obtained by replacing $X_g[k_g]$ in (15) by $X'[k_g]$. Thus,

$$Y[k_g]=\underbrace{\frac{\sqrt{N}G_{\mathrm{E}}K_{[\mathrm{sq}]}L}{2\,G}X'[k_g]}_{\text{Useful Signal Term}}+\underbrace{W[k_g]}_{\text{Noise Term}}.\tag{23}$$

The useful signal power for C-SW-SO-OFDM is obtained as

$$\sigma^2_{\mathrm{CSW}}[k]=\frac{N}{4}\left(\frac{G_{\mathrm{E}}K_{[\mathrm{sq}]}L}{G}\right)^2\mathrm{E}\left[|X'[k_g]|^2\right].\tag{24}$$

To maximize the M-QAM constellation energy and the minimum Euclidean distance, the maximum possible value of 2 for $|X_{\mathrm{D}}[l]|$ is assigned to the highest-energy QAM symbols (located at the vertices of the QAM constellation). In this case, for square M-QAM constellations, the mean square value of $X'[k_g]$ can be

computed as

$$\mathrm{E}\left[\left|X'[k_g]\right|^2\right] = \frac{4}{3}\frac{\sqrt{M}+1}{\sqrt{M}-1}. \tag{25}$$

Hence, by substituting for $\mathrm{E}[|X'[k_g]|^2]$ from (25) into (24) and substituting $K_{[\mathrm{sq}]} = 4\,C/\pi$, the useful signal power follows as,

$$\sigma^2_{\mathrm{CSW}}[k_g] = \frac{16N}{3}\frac{\sqrt{M}+1}{\sqrt{M}-1}\left(\frac{G_{\mathrm{E}}LC}{\pi G}\right)^2. \tag{26}$$

Under the assumptions of a flat channel and white noise, the useful signal power is independent of the subcarrier index k, and thus the index k can be dropped. Then, the SNR of the C-SW-SO-OFDM is given by

$$\mathrm{SNR}_{\mathrm{CSW}} = \frac{\sigma^2_{\mathrm{CSW}}}{\sigma^2_W} = \frac{16N}{3}\frac{\sqrt{M}+1}{\sqrt{M}-1}\left(\frac{G_{\mathrm{E}}LC}{\pi G\sigma_W}\right)^2. \tag{27}$$

For square M-QAM constellations, the overall BER for C-SW-SO-OFDM can be written as [34]

$$P_{\mathrm{e}[CSW]} = \frac{2\left(\sqrt{M}-1\right)}{\sqrt{M}\log_2 M}\mathrm{erfc}\left(\sqrt{\frac{3\cdot\mathrm{SNR}_{\mathrm{CSW}}}{2\,(M-1)}}\right). \tag{28}$$

E. BER of Single-Carrier SO-OFDM

Single-carrier SO-OFDM introduced in [12] as a special case of SO-OFDM, where a single OFDM data subcarrier is modulated per LED group (i.e., $\epsilon = 1$ in [12]). This special case of SO-OFDM bears many similarities to SW-SO-OFDM. Both techniques have the same OFDM subcarrier structure, but SW-SO-OFDM uses square-wave carriers instead of sinusoidal carriers and has a less complex transmitter architecture. For that reason, it is of particular interest to compare the proposed SW-SO-OFDM technique to single carrier SO-OFDM in terms of the BER performance.

An analytical BER formula for SO-OFDM was obtained in [12] using a Gaussian model for the time-domain OFDM signal and Bussgang's model [35] for clipping. However, these models are not accurate when each LED group modulates a single carrier. In this paper, a different approach is followed considering that detection is performed on the fundamental component only.

Using PSK modulation on subcarriers, the group OFDM time-domain signal for single-carrier SO-OFDM before clipping is

$$x_{g[\mathrm{sin}]}(t) = A\cos\left(2\pi k_g f_0 t + \phi_g[k_g]\right). \tag{29}$$

Following the same analysis procedure outlined in this section, a BER formula can be obtained for single-carrier SO-OFDM, where each OFDM time-domain symbol, before clipping, is a sinusoidal wave. In this case the SNR is given as

$$\mathrm{SNR}_{[\mathrm{sin}]}[k] = \frac{\sigma^2[k]}{\sigma^2_W} = \frac{N\left(G_{\mathrm{E}}K_{[\mathrm{sin}]}L/G\right)^2}{4\sigma^2_W}, \tag{30}$$

where $K_{[\mathrm{sin}]}$ is the fundamental coefficient of the Fourier series expansion of the time-domain OFDM signal. In case of no clipping (i.e., $A \le C$), $K_{[\mathrm{sin}]} = A$, whereas if $A > C$,

$$K_{[\mathrm{sin}]} = A - \frac{2\,A}{\pi}\cos^{-1}(C/A) + \frac{2\,C}{\pi A}\sqrt{A^2 - C^2}. \tag{31}$$

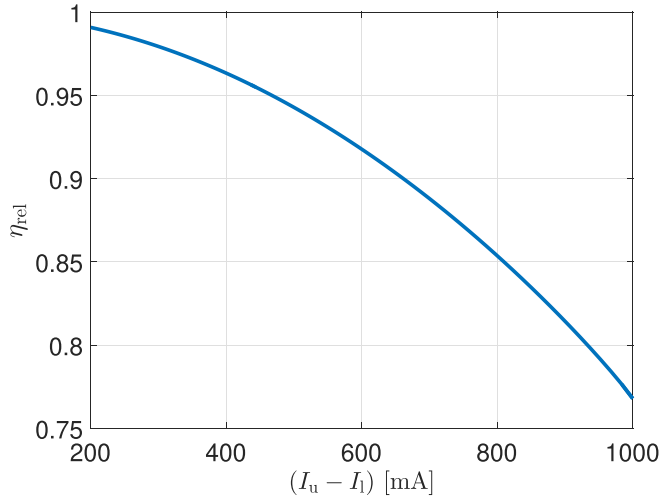

Fig. 5. Relative luminous efficacy vs. dynamic range for SW-SO-OFDM.

Notice that, as $A \to \infty$, the signal approximates a 50% duty-cycle square wave with amplitude C, and hence $\lim_{A\to\infty} K_{[\mathrm{sin}]} = 4\,C/\pi$. The analytical BER formula can be obtained by replacing $\mathrm{SNR}_{[\mathrm{sq}]}[k]$ in (18) with $\mathrm{SNR}_{[\mathrm{sin}]}[k]$, and is used to plot the analytical BER curves for single-carrier SO-OFDM in Section IV.

F. Luminous Efficacy Considerations for SW-SO-OFDM

For SW-SO-OFDM, the relative luminous efficacy, η_{rel}, can be computed for different values of the dynamic range $(I_{\mathrm{u}} - I_{\mathrm{l}})$. Therefore, in Fig. 5, η_{rel} is plotted vs. the dynamic range $(I_{\mathrm{u}} - I_{\mathrm{l}})$. From Fig. 5, it can be observed that increasing the upper and lower levels of the square-wave signal leads to a reduction in the luminous efficacy. The plot in Fig. 5 serves as a design tool for indoor VLC systems. Given a recommended maximum value for the luminous efficacy loss due to modulation, the dynamic range for SW-SO-OFDM can be directly determined from the plot.

Since square waves are well approximated by clipped sinusoids with amplitudes that are very large compared to the clipping level, the rightmost side of the contour plots in Fig. 1 represent the relative luminous efficacy (η_{rel}) for SW-SO-OFDM (i.e., large σ_g) permitting comparison with SO-OFDM. Notice that for a given dynamic range $I_{\mathrm{u}} - I_{\mathrm{l}}$, η_{rel} increases as σ_g is decreased, since the clipping distortion becomes less severe and the signal appears more sinusoidal (SO-OFDM). Section IV presents a comparison of SO- and SW-SO-OFDM when operating at the same η_{rel}.

IV. Simulation Results

In this section, the BER performance of SW-SO-OFDM, including both the uncoordinated and coordinated variants, is compared against existing OFDM techniques used for VLC, i.e., DCO-OFDM and SO-OFDM with $\epsilon = 1$, using the MATLAB simulation software [36].

The transmitter/receiver specifications and channel parameters are are listed in Table II and are taken from estimates from

TABLE II
SIMULATION PARAMETERS

Lambertian order m	1
Area of the detector A	1 cm^2
Gain of the Optical Concentrator g	3
Gain of the Optical Filter T_S	1
Responsivity R	0.28 A/W
Noise power spectral density N_0	10^{-16} mA^2/Hz
Receiver bandwidth B	20 MHz

practical channels as reported in [12] and [28]. The receiver is assumed to be oriented so that the optical axis coincides with the luminaire and the distance between the individual LEDs is considered negligibly smaller than the distance between the luminaire and the receiver photodetector, so that the channel between each LED and the photodetector is the same and the angle of incidence $\psi = 0$.

Consider an illumination system that consists of L LEDs. For SW-SO-OFDM with FFT size N, the LED group size is chosen to be $G = \lfloor \frac{N}{3} \rfloor$ and each LED group has two LEDs for coordination. To guarantee subcarriers k_1 to k_G are free from inter-carrier interference (ICI), let the first effective subcarrier for SW-SO-OFDM, $k_1 = \lceil \frac{N}{6} \rceil$ so that its first harmonic is located at subcarrier $k_G + 1$. The VLC channel is modeled as a flat channel for the small number of subcarriers used in the simulations. However, it is straightforward to extend the results to the case of non-flat channels where the use of channel estimation and equalization is necessary and well-known for OFDM systems. In following simulations, the error performance of the proposed SW-SO-OFDM schemes is evaluated versus the received optical signal-to-noise ratio (OSNR), defined as

$$\text{OSNR} = \frac{RP_{\text{R}}}{\sigma_w}. \tag{32}$$

Various modulation orders are considered as well as two FFT sizes, $N = 36$ and $N = 128$. For comparison, the performance of DCO-OFDM and SO-OFDM [12] with FFT size N and a QPSK constellation ($M = 2$) are also simulated. Recall that SO-OFDM is sine-wave based spatial combination that transmits one subcarrier per LED group. It is worth noting that both DCO-OFDM and SO-OFDM make use of $\frac{N}{2} - 1$ effective subcarriers, which is more than those in SW-SO-OFDM (due to avoidance of ICI). In our simulations, for a fair comparison regarding illumination level, we fix $N = L + 2$ for all three tested schemes (DCO-, SO-, and SW-SO-OFDM), where the unused LEDs in SW-SO-OFDM are used solely for illumination. For example, given $L = 36$, we have $N = 38$ and the number of effective subcarriers (group size G) in SW-SO-OFDM is $G = 12$, then 24 LEDs are data-carrying while the other 12 LEDs are for illumination. Such scenarios arise in small scale illumination applications. In contrast, for $N = 128$, a minimum of $L = 126$ LEDs are required. Such a large number of LEDs is available in many indoor widespread illumination scenarios requiring VLC as well as for luminaires composed of arrays of micro-LEDs [25], [28].

The dynamic range of the LED is set to 500 mA, and the full dynamic range is used in all simulations unless stated otherwise.

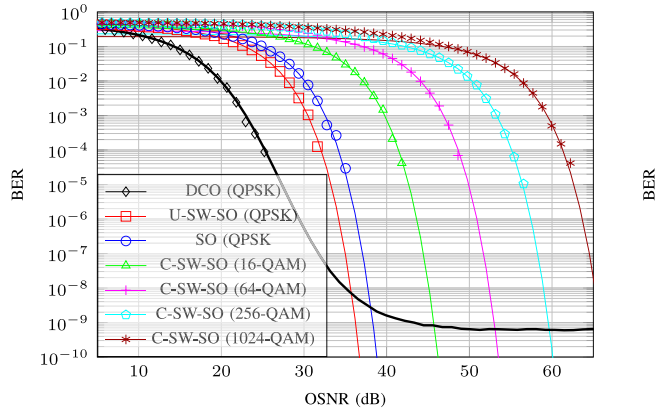

(a) N=36

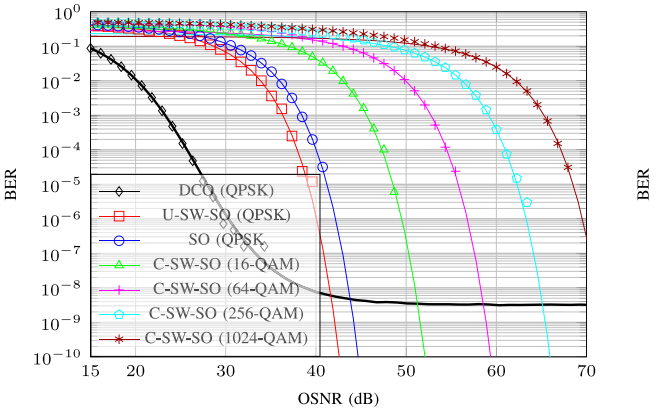

(b) N=128

Fig. 6. Probability of error comparison between the proposed SW-SO-OFDM technique, including both the uncoordinated and coordinated transmitted cases, the conventional DCO-OFDM, and SO-OFDM with $\epsilon = 1$. Continuous-line plots are the result of the analytical approximations in (19), (28), and in [12] for DCO-OFDM.

Symmetric clipping is also used, so that the clipping levels are $I_{\text{u}} = -I_{\text{l}} = 250$ mA.

In the first simulation, the group signal standard deviation, σ_g, is set to $250/\sqrt{2}$ mA, for DCO-OFDM and SO-OFDM with $\epsilon = 1$. This sets the peak-to-peak value of the SO-OFDM sinusoidal signal to 500 mA, which is the full dynamic range of the LED. Similarly, for SW-SO-OFDM, the high and low levels of the square wave are I_{u} and I_{l}, respectively. The BER is obtained via Monte-Carlo simulations and plotted vs. SNR in Fig. 6 for DCO-OFDM, SO-OFDM with $\epsilon = 1$, and the proposed U-SW-SO-OFDM and C-SW-SO-OFDM. The modulation used on subcarriers for all signaling techniques is 4-QAM, except for C-SW-SO-OFDM which uses 16-, 64-, 256-, and 1024-QAM.

The results show that DCO-OFDM performs better than all other approaches based on group modulation at low SNRs. As shown and discussed in [12], this due to DCO-OFDM having a higher useful signal power and that the dominant source of noise at low SNR is the channel AWGN, not the NLD noise. However, as the channel SNR increases, the NLD becomes the dominant source of noise and since DCO-OFDM has a high PAPR, and hence less immunity to NLD noise, the BER saturates and

stops decreasing significantly with increasing SNR. This also shows that, despite the small number of modulated DCO-OFDM subcarriers in the simulation, the detrimental effects of PAPR and NLD noise are still significant at high SNRs. The BER performance degradation is even more significant for a larger number of subcarriers, and the use of SO-OFDM and its lower-complexity variant, SW-SO-OFDM would be even more justified. For SO-OFDM with $\epsilon = 1$ and SW-SO-OFDM, clipping causes only attenuation of the signal as the fundamental term of the Fourier Series expansion is affected by clipping. The signal obtained by clipping a periodic waveform is a periodic waveform with an attenuated fundamental frequency component. It can be seen from Fig. 6 that the proposed U-SW-SO-OFDM outperforms SO-OFDM in terms of probability of error. This is due to the fact that the fundamental coefficient of the Fourier Series expansion (6), is $K_{[\text{sq}]} = 4\,C/\pi$, while for SO-OFDM with $\epsilon = 1$ using the full dynamic range without clipping, it is $K_{[\text{sin}]} = C$, as discussed in Section III-A. This corresponds to an SNR advantage of 2.10 dB as discussed in Section III, and as evident from the BER results in Fig. 6.

In the second simulation, the SW-SO-OFDM system is compared to SO-OFDM with $\epsilon = 1$ at the same relative efficacy loss. With a dynamic range of 500 mA, and a target relative luminous efficacy of 95%, a signal standard deviation of 745 mA is required for SO-OFDM, as computed from Fig. 1, and is also used for DCO-OFDM. For SW-SO-OFDM, from Fig. 5, the value of $I_{\text{u}} - I_{\text{l}}$ that corresponds to a relative luminous efficacy of 95% is 467 mA. This means that the full dynamic range of the LED (500 mA) is not used. The BER vs. SNR is plotted in Fig. 7.

The BER results in Fig. 7 show that DCO-OFDM suffers from a high BER floor due to significant clipping distortions while the (SW-)SO-OFDM schemes are shown to be immune to the clipping distortions. It is also shown that the U/C-SW-SO-OFDM schemes perform the same as in Fig. 6 though under a different relative efficacy. Notice that SO-OFDM with $\epsilon = 1$ achieves a better performance, approaching U-SW-SO-OFDM, since the peak clipping helps to shape the sinusoidal waves to approximate square waves. This observation justifies $\lim_{A\to\infty} K_{[\text{sin}]} = 4\,C/\pi$. Though the performances of U-SW-SO-OFDM and SO-OFDM are comparable, the complexity of U-SW-SO-OFDM is much lower. Specifically, it is important to note that each group in U-SW-SO-OFDM does not require a high-speed DAC or DPD as compared to the case of the SO-OFDM transmitter.

V. Experimental Results

In this section, an experimental demonstration of the C-SW-SO-OFDM VLC transmitter is described. As a proof-of-concept of C-SW-OFDM based on the spatial summing architecture, binary-level signals from two LEDs are combined in space to transmit a single complex QAM symbol. The subcarrier is modulated using 64-QAM modulation, which shows experimentally that the proposed SW-SO-OFDM can be extended to higher-order/multi-level constellations, by coordinating the transmission of 2 LEDs, as described for C-SW-SO-OFDM in

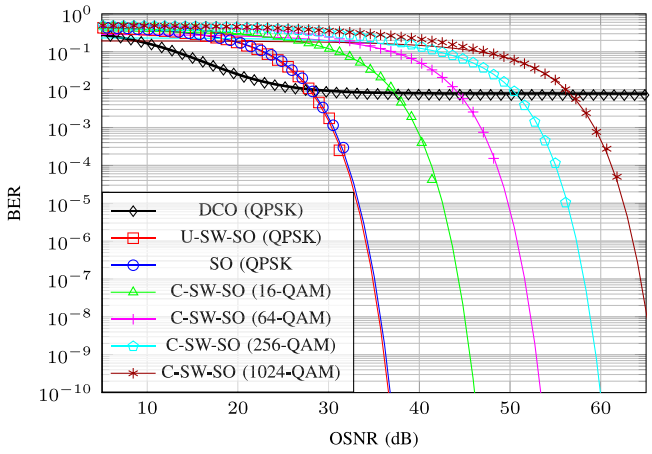

(a) N=36

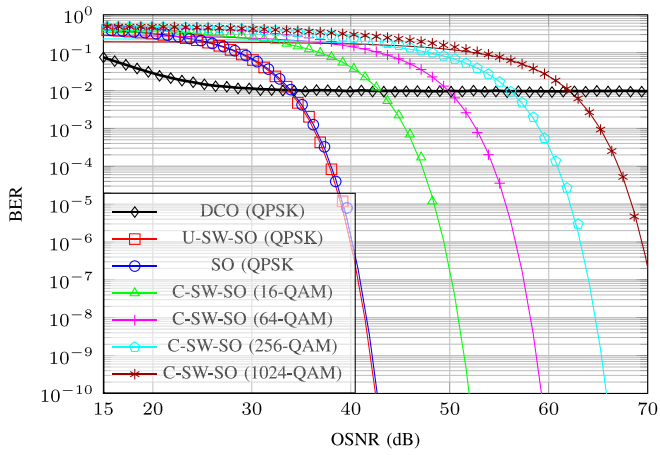

(b) N=128

Fig. 7. Probability of error comparison between the proposed SW-SO-OFDM technique, including both the coordinated and uncoordinated scenarios, the conventional DCO-OFM, and SO-OFDM with $\epsilon = 1$, at the same relative luminous efficacy $\eta_{\text{REL}} = 95\%$. Continuous-line plots are the result of the analytical approximations in (19), (28), and in [12] for DCO-OFDM.

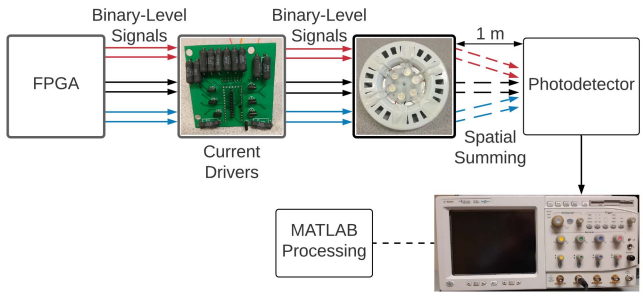

Fig. 8. Block diagram showing the coordinated SW-SO-OFDM experimental setup. Although 3 pairs of LEDs are shown in the figure as the luminaire used has 6 LEDs, only one pair is modulated in the experiment as a proof-of-concept.

Section III-D. Fig. 8 depicts the functional block diagram of the transmitter and receiver used to demonstrate C-SW-SO-OFDM.

The transmitter modulation circuit is implemented with the Altera Cyclone IV FPGA DE2-115 development board produced by Terasic. Data is generated using a 20-bit linear finite shift register (LFSR). The taps of the register is set to 1st, 3rd, 4th,

and 6th bit of the registers. The LFSR is capable of generating 2^{20} or approximately 1 million unique values before repeating. A subset of the LFSR is then used as the data to the LED controller. A data file is generated on a computer and loaded into the on-board memory of the FPGA. For simplicity, each data stream is modulated onto a single square-wave carrier, implemented as a set of counters. The main clock of the controller is based upon the on-board oscillator set to 50 MHz, and is used as the reference clock. The controller symbol period is set to 130.2 kilosymbols per second, resulting in a data rate of 781.25 kbps. This is achieved by clock division of the 50 MHz clock by 384 clock cycles. The controller operates the coordinated LED pair. The wave address is controlled by a 400 MHz clock generated through a phase lock loop. This clock is then used in clock division to generate the required carrier frequency. While the demonstrated data rate of 781.25 kbps is relatively low, it can be increased by using a larger number of LEDs and subcarriers (in the hundreds), as is typically used in practical VLC scenarios. In addition, the data rate can be increased by using LEDs with a larger bandwidth and advanced synchronization techniques at the receiver. Note that the experimental demonstration presented in this paper serves only as a proof-of-concept for the spatial summing architecture and the low-complexity transmitter using square-waves as carriers. Further experimental demonstrations in more practical settings achieving larger data rates are the subject of future research.

The carrier frequency is set to 781.25 kHz. The frequency is calculated based upon three factors. The first is that the carrier frequencies must be an even harmonic of the symbol frequency which is 130.2 kilosymbols per second. The value of 781.25 kHz corresponds to the 6th harmonic of symbol frequency. Secondly, in a typical setting where many subcarriers are modulated, the harmonics of the carrier frequency can not overlap each other to reduce error. The harmonics of the used carrier frequency (781.25 kHz) are located at 2343.75 kHz and 3906.25 kHz for the 3rd and 5th harmonic, respectively. As discussed in Section III, these carrier frequencies should be unused for data transmission to avoid ICI. Alternatively, successive interference cancellation [37] can be used to eliminate the interference, allowing the use of more OFDM subcarriers for data transmission, and thereby increasing the overall bandwidth efficiency. Lastly the frequency must be achievable using discrete clock division. The used carrier frequency is achieved through a clock divisor using 400 MHz clock. The value used is set to 4 clock ticks.

The binary/square-wave carrier signal then modulates the intensity of a high power Philips Lumileds Luxeon Rebel LXML-PWN1-0100 LED using two independent current drivers. The white light component of the LXML-PWN1-0100 has an optical 3 dB bandwidth of approximately 2 MHz, a maximum continuous current of 1 A, a typical forward voltage of 3.2 V and a luminous efficacy of 80 lm/W at 700 mA. Each LED is driven with an average current of 400 mA and 100% modulation depth.

As shown in Fig. 8, the signals from both LEDs sum in space and are detected at the receiver placed at 1 m from the transmitter. The receivers analog front end is implemented using the Thorlabs PDA 36 A variable gain amplified photo diode directly coupled to an Agilent Infiniium 54855 DSO oscilloscope. The PDA 36 A is configured to operate with a 10 dB gain and bandwidth of 5 MHz. The oscilloscope then samples the waveform at 10 Msps and is capable of producing binary data files of 16 Mpts. To guarantee synchronization, the oscilloscope also probes a synchronization signal generated on the FPGA directly through an auxiliary cable. The synchronization signal is a delayed clock signal whose edges mark the start of each OFDM frame.

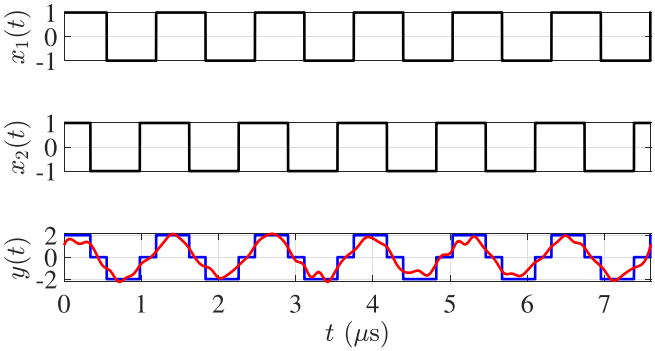

Fig. 9. Time-Domain waveforms of C-SW-SO-OFDM. The binary-level signals of both LEDs are shown in the first two subplots, while their sum (blue) is compared to the experimental received signal (red) in the bottom subplot.

Demodulation of the received signal is performed by post processing using MATLAB [36]. First, the start and the end of each OFDM time-domain symbol are identified with the help of the synchronization signal. Each OFDM symbol is then separated and processed individually. The frequency-domain OFDM symbols are obtained by using FFT demodulation. Since the modulation bandwidth of the LED is smaller than the inverse of the maximum excess delay of the non-line-of-sight (NLoS) signal component, the multipath effect is negligible, resulting in no ISI, and the VLC channel is considered flat for the narrowband fundamental-frequency signal [28], [38]. Therefore, in this particular scenario the use of a CP is unnecessary and single-tap channel equalization is used to obtain the received QAM constellation data symbols. Finally, bit detection and BER computation are performed.

Fig. 9 shows sample waveforms for a single OFDM symbol. The first and second subplots show the binary/square-wave transmitted signals of the first ($x_1(t)$) and second ($x_2(t)$) LEDs. The third subplot compares the sum $x_1(t) + x_2(t)$ (shown in blue) to the experimental received signal $y(t)$ (shown in red). It can be noticed that, due to the the lowpass frequency response of the LED [28], the higher order harmonics of the transmitted square-wave signals are attenuated, and the received signal resembles a sinusoidal wave. For multiple subcarriers, the received signal resembles the sum of sinusoidal signals, each corresponding to a particular OFDM subcarrier, i.e. a full OFDM signal is received by the photodetector. This allows for the use of a conventional OFDM receiver.

Fig. 10 depicts the measured constellation. It is clear from Fig. 10 that the *post-detection SNR* (27.5 dB) in this experiment is large enough to cause a near zero symbol error rate over the 13,617 measured symbols. While it remains clear that the carriers sum optically in space, these results successfully demonstrate

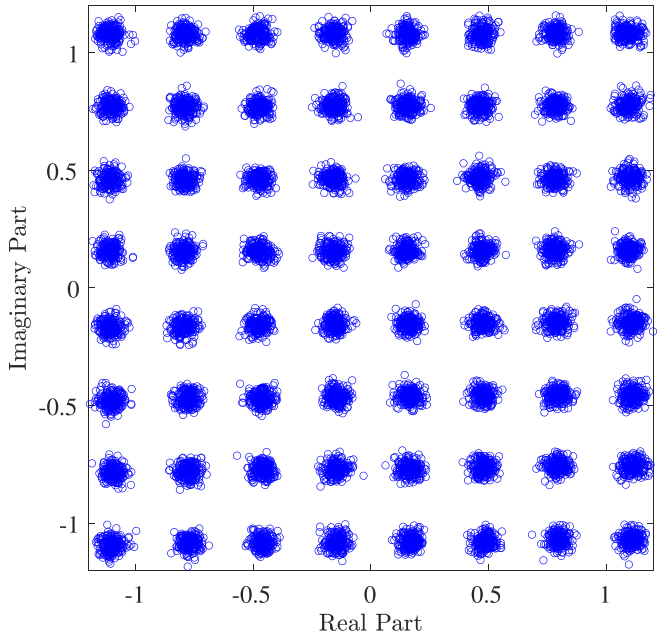

Fig. 10. Experimental received 64-QAM constellation. A total of 13,617 QAM symbols are shown. The high calculated SNR of 27.5 dB results in a zero symbol-error rate over this number of QAM symbols.

the concept of C-SW-SO-OFDM based on spatial summing in an experimental framework. The error vector magnitude (EVM) can be computed as [39],

$$\text{EVM}\ (\%) = \sqrt{\frac{\text{E}\left[|Y-X|^2\right]}{\text{E}\left[|X|^2\right]}} \times 100\%, \tag{33}$$

where X and Y denote the target and received QAM constellation point, respectively. In this experimental demonstration, an EVM value of 4.27% is reported.

This experimental demonstration shows that we were able, for the first time in literature to our knowledge, to produce an OFDM symbol by summing two binary signals in space, which was detected using a conventional OFDM receiver.

VI. Conclusion

This paper presents square-wave spatial optical OFDM (SW-SO-OFDM) which combines spatial summing with a simple transmitter architecture. The new technique combines the high spectral efficiency, robustness against multipath effects, and simple equalization of OFDM systems, with the low PAPR and immunity to nonlinear effects of SO-OFDM, while avoiding the complex transmitter architecture of SO-OFDM. This is achieved by modulating the LEDs with binary-level signals, thereby eliminating the need for DPDs and DACs. This also allows for the use of energy-efficient power drivers. In addition, coordinated SW-SO-OFDM (C-SW-SO-OFDM) was proposed to allow for multi-level QAM signaling.

A BER analysis of SW-SO-OFDM techniques, as well as BER simulations, show their superior performance compared to SO-OFDM with one subcarrier per LED group when the full dynamic range of the LED is used. Moreover, the proposed techniques are more resilient to NLD given they have only two amplitude levels. To validate our work, the multi-level technique was implemented experimentally by transmitting a 64-QAM signal by coordinating the transmission of 2 LEDs driven by binary-level signals, over a distance of 1 m and were able to successfully demodulate the signal at a receiver SNR of 27.5 dB. The components used in the experimental demonstration are inexpensive and off-the-shelf. That is, SW-SO-OFDM can realize VLC systems with a similar total data rate as conventional optical OFDM while using simple binary emissions. In contrast to conventional DCO-OFDM VLC systems, SW-SO-OFDM does not require a high-speed DAC or non-linear distortion compensation. However, a drawback of SW-SO-OFDM is that though the modulation circuitry and a current driver are simple they are must be implemented for each LED group as opposed to a single high-current driver for all LEDs in conventional systems. In addition, in SW-SO-OFDM the number of required LEDs is linked to the number of modulated subcarriers, which constitutes a trade-off between the overall system bit-rate and the system complexity in some application scenarios where a large number of LEDs is not required for illumination.

Future work includes further increases the bandwidth efficiency by considering the modulation of multiple subcarriers per LED, and/or by modulating the odd-harmonic subcarriers and using successive interference cancellation (SIC) techniques to eliminate the resulting inter-carrier interference. Also, the optimization of the subset of subcarriers of each LED to be modulated to minimize the PAPR should be considered. Finally, the experimental work in this paper can be extended to implement a larger number of LEDs and OFDM subcarriers over a variety of ranges as well as measuring the impact of illumination dimming.

Appendix
Optimality of Square-Wave Signals

In the appendix, the optimality of square-wave signals is shown in the sense that they achieve the highest fundamental frequency component among all periodic signals restricted to a dynamic range between $-C$ and C. For simplicity, and without loss of generality, the proof is given for even functions, however, the result is also valid for an arbitrary time shift.

Theorem 1: Define $\mathcal{P}$ as the set of zero-mean, even, and periodic carrier signals with period T, such that $-C \le p(t) \le C$. The $p^*(t) \in \mathcal{P}$ that maximizes the fundamental coefficient of the Fourier Series expansion, $a_1 = \frac{2}{T}\int_{-T/2}^{T/2} p(t)\cos(2\pi f_0 t)dt$, is

$$p^*(t) = \begin{cases} C & |t| \le T/4 \\ -C & |t| > T/4 \end{cases} \tag{34}$$

for $-T/2 \le t < T/2$.

Proof: The optimization problem is formulated as follows:

$$\begin{aligned} \underset{p\in\mathcal{P}}{\text{maximize}} \quad & a_1 = \frac{2}{T}\int_{-T/2}^{T/2} p(t)\cos(2\pi f_0 t)dt \\ \text{subject to} \quad & -C \le p(t) \le C \end{aligned}$$

We have

$$a_1 \leq \frac{2}{T}\int_{-T/2}^{T/2} |p(t)|\,|\cos(2\pi f_0 t)|\,dt$$
$$\leq \frac{2C}{T}\int_{-T/2}^{T/2} |\cos(2\pi f_0 t)|\,dt, \quad (35)$$

with equality for the 50% duty-cycle cycle square wave $p^*(t)$. □

REFERENCES

[1] L. Grobe et al., "High-speed visible light communication systems," *IEEE Commun. Mag.*, vol. 51, no. 12, pp. 60–66, Dec. 2013.

[2] I. L. Azevedo, M. G. Morgan, and F. Morgan, "The transition to solid-state lighting," *Proc. IEEE*, vol. 97, no. 3, pp. 481–510, Mar. 2009.

[3] T. Cevik and S. Yilmaz, "An overview of visible light communication systems," in *Proc. Int. J. Comput. Netw. Telecommun.*, vol. 7, no. 6, Nov. 2015, pp. 139–150.

[4] J. M. Kahn and J. R. Barry, "Wireless infrared communications," *Proc. IEEE*, vol. 85, no. 2, pp. 265–298, Feb. 1997.

[5] R. Mesleh, R. Mehmood, H. Elgala, and H. Haas, "Indoor MIMO optical wireless communication using spatial modulation," in *Proc. IEEE Int. Conf. Commun.*, 2010, pp. 1–5.

[6] M. Z. Afgani, H. Haas, H. Elgala, and D. Knipp, "Visible light communication using OFDM," in *Proc. IEEE 2nd Int. Conf. Testbeds Res. Infrastructures Develop. Netw. Communities*, 2006, pp. 1–6.

[7] C. Lin, Y. Chi, C. Tsai, H. Chen, and G. Lin, "Two-color laser diode for 54-Gb/s fiber-wired and 16-Gb/s MMW wireless OFDM transmissions," *Photon. Res.*, vol. 5, no. 4, pp. 271–279, Aug. 2017.

[8] K. Mallick et al., "Cyclic prefix length optimization in OFDM-MMWOF/PAM4-FSO integrated system for future generation smart wireless communication," *Opt. Quantum Electron.*, vol. 55, no. 64, pp. 658–665, 2023.

[9] J. Armstrong and B. J. C. Schmidt, "Comparison of asymmetrically clipped optical OFDM and DC-biased optical OFDM in AWGN," *IEEE Commun. Lett.*, vol. 12, no. 5, pp. 343–345, May 2008.

[10] Z. Yu, R. J. Baxley, and G. T. Zhou, "Distributions of upper PAPR and lower PAPR of OFDM signals in visible light communications," in *Proc. IEEE Int. Conf. Acoust., Speech, Signal Process.*, 2014, pp. 355–359.

[11] J. Sheu, B. Li, and J. Lain, "LED non-linearity mitigation techniques for optical OFDM-based visible light communications," *IET Optoelectron.*, vol. 11, no. 6, pp. 259–264, 2017.

[12] M. S. A. Mossaad, S. Hranilovic, and L. Lampe, "Visible light communications using OFDM and multiple LEDs," *IEEE Trans. Commun.*, vol. 63, no. 11, pp. 4304–4313, Nov. 2015.

[13] G. del Campo-Jimenez, F. J. Lopez-Hernandez, and R. Perez-Jimenez, "Modulation schemes effect on the driver efficiency and the global VLC transmitter energy consumption," in *Proc. IEEE 10th Int. Symp. Commun. Syst., Netw. Digit. Signal Process.*, 2016, pp. 1–6.

[14] M. S. A. Mossaad and S. Hranilovic, "Practical OFDM signalling for visible light communications using spatial summation," in *Proc. IEEE 27th Biennial Symp. Commun.*, 2014, pp. 5–9.

[15] H. Dong, H. Zhang, K. Lang, B. Yu, and M. Yao, "OFDM visible light communication transmitter based on LED array," *Chin. Opt. Lett.*, vol. 12, no. 5, May 2014, Art. no. 052301.

[16] A. F. Hussein and H. Elgala, "Lightweight multi-carrier modulation for IoT," *Proc. SPIE*, vol. 10559, pp. 183–192, 2018.

[17] F. B. Ogunkoya, W. O. Popoola, and S. Sinanović, "Pilot-assisted PAPR reduction technique for O-OFDM using multiple LEDs in VLC systems," in *Proc. IEEE Int. Conf. Commun. Workshops*, 2016, pp. 309–314.

[18] J. Du, W. Xu, H. Zhang, and C. Zhao, "Visible light communications using spatial summing PAM with LED array," in *Proc. IEEE Wireless Commun. Netw. Conf.*, 2017, pp. 1–6.

[19] M. Kong et al., "Underwater wireless optical communication using an arrayed transmitter/receiver and optical superimposition-based PAM-4 signal," *Opt. Exp.*, vol. 26, no. 3, pp. 3087–3097, Feb. 2018.

[20] Z. Ghassemlooy, F. Ebrahimi, S. Rajbhandari, S. Olyaee, X. Tang, and S. Zvanovec, "Visible light communications with hybrid OFDM-PTM," in *Proc. IEEE 13th Int. Wireless Commun. Mobile Comput. Conf.*, 2017, pp. 894–898.

[21] G. J. M. Forkel and P. A. Hoeher, "Constrained intensity superposition: A hardware-friendly modulation method," *J. Lightw. Technol.*, vol. 36, no. 3, pp. 658–665, Feb. 2018.

[22] G. J. M. Forkel and P. A. Hoeher, "Amplitude modulation by superposition of independent light sources," in *Proc. IEEE 12th Int. Joint Conf. e- Bus. Telecommun.*, 2015, pp. 29–35.

[23] L. Deniel et al., "DAC-less PAM-4 generation in the o-band using a silicon Mach-Zehnder modulator," *Opt. Exp.*, vol. 27, pp. 9740–9748, 2019.

[24] Y. Yang et al., "Low complexity OFDM VLC system enabled by spatial summing modulation," *Opt. Exp.*, vol. 27, no. 21, pp. 30788–30795, Oct. 2019.

[25] T. Komine and M. Nakagawa, "Fundamental analysis for visible-light communication system using LED lights," *IEEE Trans. Consum. Electron.*, vol. 50, no. 1, pp. 100–107, Feb. 2004.

[26] P. Lumileds, "Power light source luxeon rebel," 2007. [Online]. Available: http://www.led-tech.de/produkt-pdf/luxeon/DS56_Rebel.pdf

[27] R. Lenk and C. Lenk, *Practical Lighting Design With LEDs*. Hoboken, NJ, USA: Wiley, 2011.

[28] J. Grubor, S. Randel, K.-D. Langer, and J. W. Walewski, "Broadband information broadcasting using LED-based interior lighting," *J. Lightw. Technol.*, vol. 26, no. 24, pp. 3883–3892, Dec. 2008.

[29] A. Narasimhamurthy, M. Banavar, and C. Tepedelenliouglu, *OFDM Systems for Wireless Communications*. San Rafael, CA, USA: Morgan & Claypool, 2010.

[30] IEEE 802.11bb task group on light communications. 2021. Accessed: Feb. 12, 2021. [Online]. Available: https://www.ieee802.org/11/Reports/tgbb update.htm

[31] O. Kükrer, H. B. Ertan, M. Y. üçtug, R. Colyer, and A. Consoli, "Modulation techniques," in *Modern Electrical Drives*. Dordrecht, The Netherlands: Springer, 2000, ch. 13, pp. 289–309.

[32] H. Chen, S. Fang, S. Feng, and C. Shen, "Method and apparatus for providing a power factor correction (PFC) compatible solution for non-sinusoidal uninterruptible power supply (UPS)," U.S. Patent 8,405,372, Mar. 26, 2013.

[33] J. G. Proakis, *Digital Communications*, 5th ed. New York, NY, USA: McGraw Hill, 2007.

[34] R. Mesleh, H. Elgala, and H. Haas, "On the performance of different OFDM based optical wireless communication systems," *IEEE/OSA J. Opt. Commun. Netw.*, vol. 3, no. 8, pp. 620–628, Aug. 2011.

[35] J. J. Bussgang, "Crosscorrelation functions of amplitude-distorted Gaussian signals," Res. Lab. Electron., Massachusetts Inst. Technol., Cambridge, MA, USA, Tech. Rep. 216, 1952.

[36] The Mathworks, Inc., Natick, MA, USA: MATLAB version 9.8.0.1323502 (R2020a), 2020. Accessed: Jan. 1, 2021. [Online]. Available: https://www.mathworks.com

[37] C. Yang et al., "Successive interference cancellation in practical indoor interfered visible light communication," in *Proc. Adv. Photon.*, 2016, Paper SpTu2F.5.

[38] H. Ma, "Coordinated transmission for visible light communication systems. Ph.D. dissertation, Univ. British Columbia, Vancouver BC, Canada, 2017.

[39] Z. Yu, R. J. Baxley, and G. T. Zhou, "On the EVM calculation of clipped optical OFDM signals," in *Proc. IEEE Photon. Soc. Summer Topical Meeting Ser.*, 2012, pp. 96–97.